NATIONAL AERONAUTICS AND SPACE ADMINISTRATION

NASA-INSTITUTE-FOR-ADVANCED-CONCEPTS-(NIAC) PHASE I

FINAL TECHNICAL REPORT ON

3D Photocatalytic Air Processor for Dramatic Reduction of Life Support Mass and Complexity

April 27, 2015

Reporting period: 07/07/14 to 04/27/2015

From

NASA Ames Research Center

Moffett Field, CA

Technical Point of Contact:

Dr. Bin Chen
Principal Investigator
Tel: 650 6040310
Fax: 650 604 6779
Email: Bin.Chen-1@nasa.gov

Co- Investigators:

Darrell Jan
Kenny Cheung
John Hogan
NASA Ames Research Center

3D Photocatalytic Air Processor for Dramatic Reduction of Life Support Mass and Complexity

Final Report for the Period of July 07, 2014 to April 27, 2015

1. Summary

To dramatically reduce the cost and risk of CO_2 management systems in future extended missions, we have conducted preliminary studies on the materials and device development for advanced "artificial photosynthesis" reaction systems termed the High Tortuosity PhotoElectroChemical (HTPEC) system. Our Phase I studies have demonstrated that HTPEC operates in much the same way a tree would function, namely directly contacting the cabin air with a photocatalyst in the presence of light and water (as humidity) to immediately conduct the process of CO_2 reduction to O_2 and useful, "tunable" carbon products. This eliminates many of the inefficiencies associated with current ISS CO_2 management systems. We have laid the solid foundation for Phase II work to employ novel and efficient reactor geometries, lighting approaches, 3D manufacturing methods and *in-house* grown novel catalytic materials.

The primary objective of the proposed work is to demonstrate the scientific and engineering foundation for light-activated, compact devices capable of converting CO_2 to O_2 and mission-relevant carbon compounds. The proposed HTPEC CO_2 management system will demonstrate a novel pathway with high efficiency and reliability in a compact, lightweight reactor architecture. The proposed HTPEC air processing concept can be developed in multiple architectures, such as centralized processing as well as "artificial leaves" distributed throughout the cabin that utilize pre-existing cabin ventilation (wind). Additionally, HTPEC can be deployed with spectrally tunable collection channels for selectable product generation. HTPEC employs light as its only energy source to remove and convert waste CO_2 using a non-toxic composite catalyst.

We have demonstrated in the Phase I studies the production, tunability and robustness of the novel composite catalysts following the preliminary work in the Chen laboratory. Additionally, we have designed, fabricated and tested all components of HTPEC device with active materials, including flow modeling to optimize flow mixing and pressure drop as well as the production of ethylene and other larger hydrocarbons. To best determine how this technology could be implemented, we also performed system integration optimization and trade studies. This includes parameters such as mass, volume, power in relation to selected mission configurations, CO_2 delivery methods and light source/delivery approaches.

The project schedule was initially delayed due to initial issues with processing of procurement funding at Ames. But with increased team efforts, we have accomplished every aspect of proposed phase I feasibility studies, and attracted collaboration from academics as well as industrial collaborators. The NIAC work has also received NASA Ames center management support with matching funds and has been managed by NASA Ames Chief Technologist Office.

2. Results and Progress

1. Device design, characterization and prototyping:

Following the Phase I proposed device concept to maximize the reaction flowing mixing and interaction time with catalysts (see **Figure 1**), we started the preliminary design work with the adaptation of traditional flow cell architectures to include two new elements: 1) high tortuosity geometry for maximization of fluid mixing, and 2) light-guide or light-producing elements. Recent work has included device design for efficient transport of light and (gas) mass.

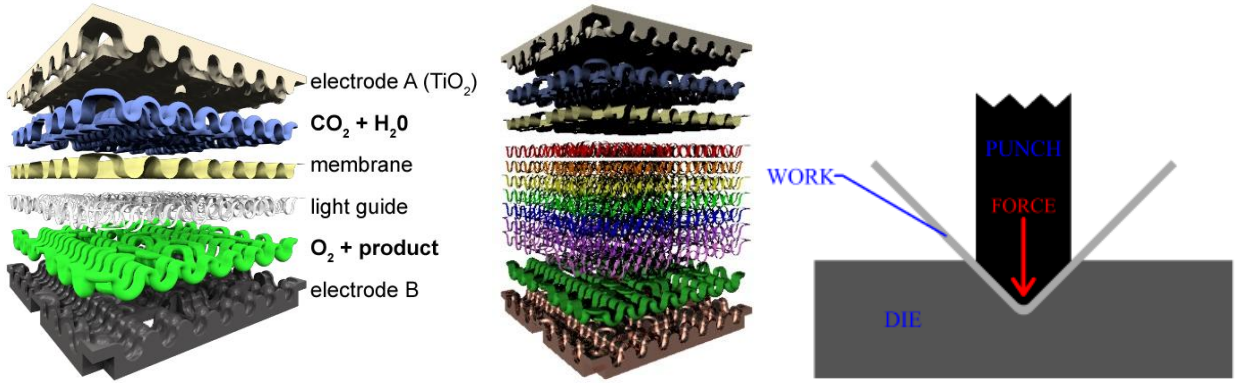

Figure 1. Proposed setup with single light guide/producing material (left), multiple wavelength/band-specific guide/producing materials (middle), using a die to control bend radius (http://thelibraryofmanufacturing.com/sheetmetal_bending.html)

Considering various fabrication techniques, we pursued a 2.5D device concept using pop-up designs of origami interleaved tube cellular materials, which allow for adjustable volume ratios, maximal interfacial surface area, and production by lamination of flat sheets. They are etched and folded into the shapes shown, which are examples of compact, space- and mass-efficient designs. Stacking the folded sheets forms tortuous pathways that can span the construction, according to the folding patterns. **Figure 2** depicts interleaved tube cellular structures manufactured by 3D printing, showing foldability in the XY directions and rigidity in the Z direction. We examined the use a type of foldable honeycomb-like structure, but differing in that the pathways are more complex and convoluted than the straight through paths in honeycomb. The foldable structure has the advantage of being more compact and sturdy during launch, and yet easily deployable in space. Normally, a foldable structure has the fluid mechanical disadvantage of having sharp corners, which cause stagnation zones where debris can build up. However, we will address this two ways. One is to use a multilayer approach, in which the inner

layer, after folding, thereby smoothing out the corner. The other is to use processes than have an inherently larger radius of curvature in the fold zones, i.e. avoid making a crease by bending around a die or form block (**Figure 1**). Such origami structures also allow us to adjust the light intensity and direction, as well as CO_2 gas flow concentrations with turn-key operation, with separate flow-able volumes on orthogonal axes by employing the following: (1) adjustable ratio with bulk deformation (2) production by lamination of flat patterned sheets (3) 3D printed prototype for tests and validations.

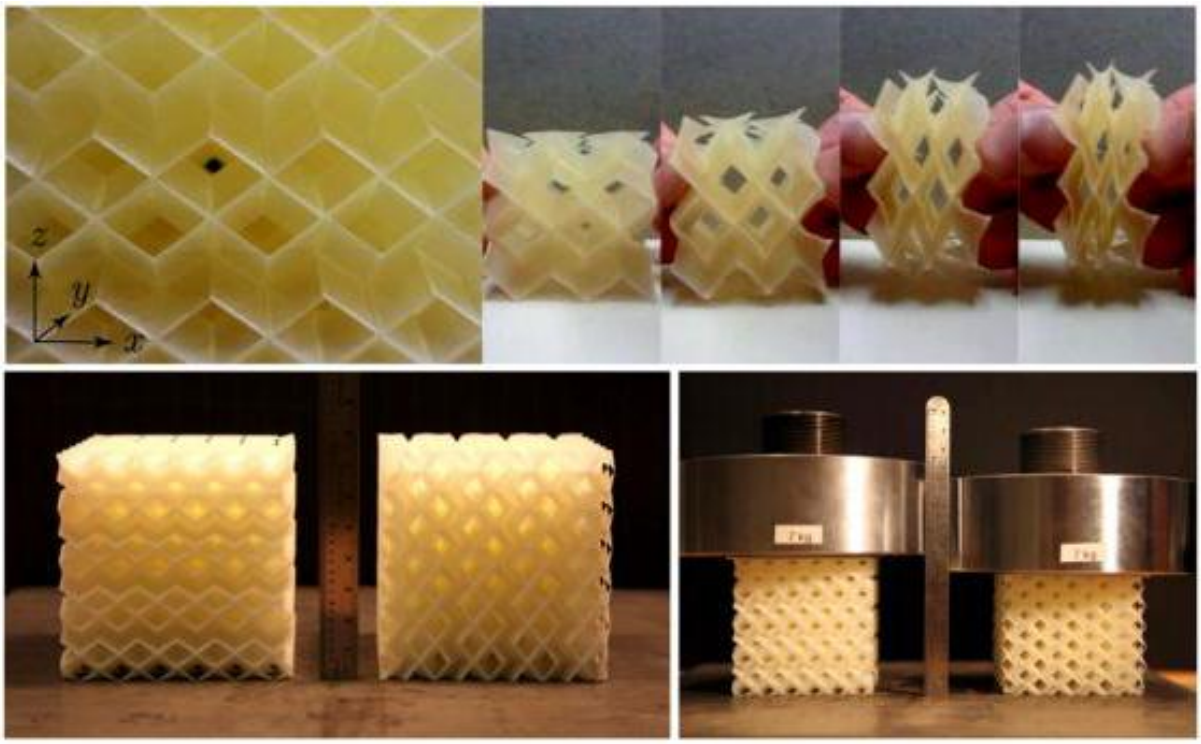

Figure 2. Interleaved tube cellular structures manufactured by 3D printing, showing foldability in XY direction (top) and rigidity in Z direction (bottom). Each of the bottom images shows two copies of the same structure, with the right-hand sample orientated so that the z axis is parallel to the basal plane, and the left-hand sample orientated so that the z axis is perpendicular to the basal plane. Initial conditions are shown in the left-hand set of images, and identical loading conditions are shown in the right-hand set of images, displaying the difference in response for the different orientations. (ref)

For the photocatalytic application, the origami shapes are created from flat sheets of transparent plastics as depicted in **Figure 3**. They are etched and folded into the shapes shown, which are examples of compact, space- and mass-efficient designs. Stacking the folded sheets forms tortuous pathways, which enhance mixing and can span the construction according to the folding patterns. Assembled volumes can maintain fold-ability, allowing the structure to be flat-folded for storage and allowing the tortuosity of the pathways to be continuously adjustable. Preliminary tests in Phase 1 have shown that the transparent material can also serve as catalyst support, and can transmit light to photolytic areas. The cylindrical shape, formed from the same

type of flat transparent sheet, demonstrates the light conducting and transmitting capability has produced assemblies which are deployable in X/Y directions, yet retain considerable strength in the Z direction once deployed. In addition to the LED lamp likely available in the cabin environment, we can use optical fiber lighting to directly deliver the solar energy to the tortuous free-space pathways.

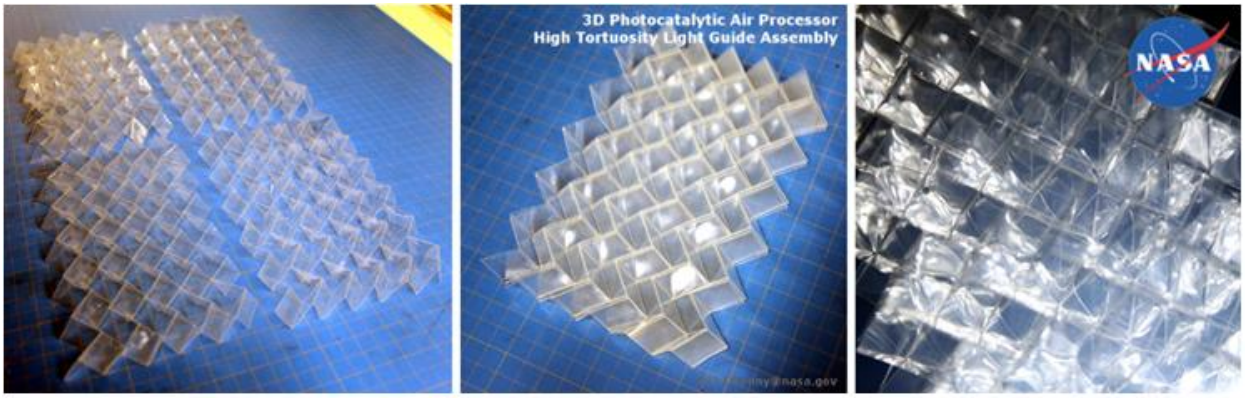

Figure 3. Transparent origami substrates for photocatalysts

Another alternative candidate that can serve as s 2.5D photocatalysis substrate is waveguide materials. In this case, we employ edge-lit technology (see **Figure 4)** currently being introduced to television and computer monitors. The edge lit material uses low refractive index structures to disperse the light, as shown in **Figure 4(a)**. The commercial sample in **Figure 4(b)** uses gas bubble structures; another approach is to etch patterns onto the surface.

We are considering bringing in solar energy using fiber optical light, or a blue LED light assembly. The LED edge-lit configuration has high energy efficiency, a small form factor, and highly efficient light distribution via perpendicular surface and uniform luminance. We plan to design the reactor in Phase II tests using the flexibility to add reflective backsides as the structure materials and possibly double-sided illuminations for both entrance and exit ports of the gas flow.

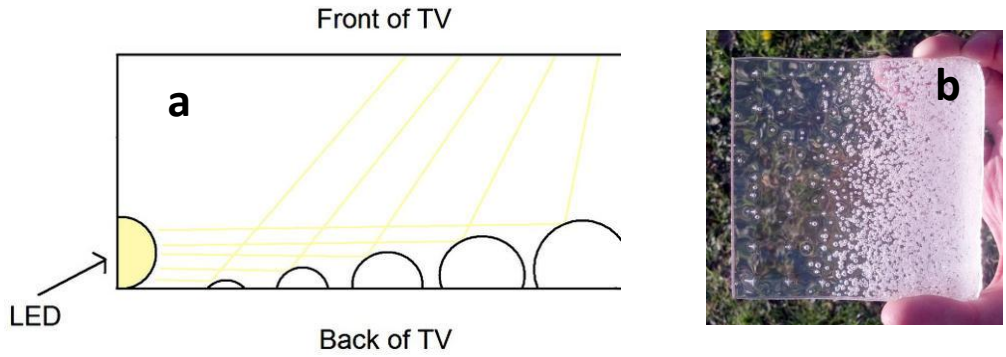

Figure 4. Edge lit technology enables small form factor and high energy efficiency. a) diagram illuminating light dispersion. b) commercial sample of edge lit materials

We are currently seeking edge-lit material in foldable thicknesses. We believe this is technically easy to achieve, and is solely a budgetary challenge. In the meantime, for test purposes, we have experimented with reshaping samples of edge-lit material using a low cost, low temperature casting technique. We have identified the commercially available waveguide material acrylite to begin the preliminary investigations. The 3 mm acrylic sheet has the same consistent transmission clarity as the clear film in the visible spectrum range (shown in **Figure 5**), making it the ideal material choice as the catalyst substrate surface to transmit the light.

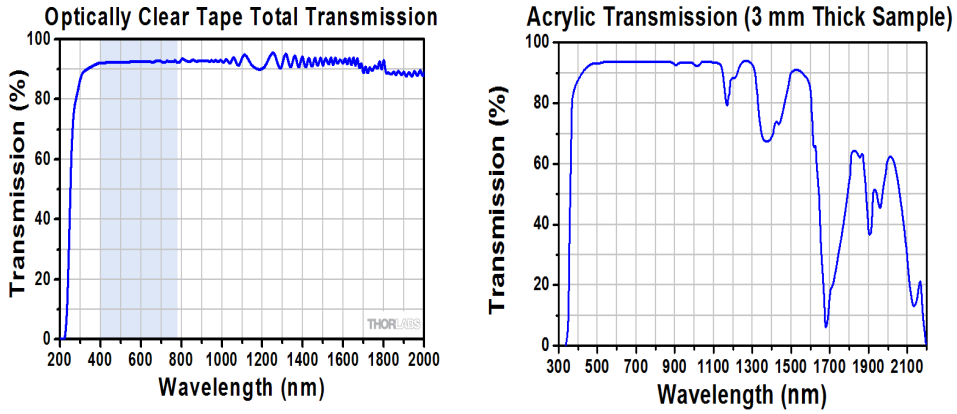

Figure 5. High transmission acrylic waveguide materials for 2.5D HTPEC device

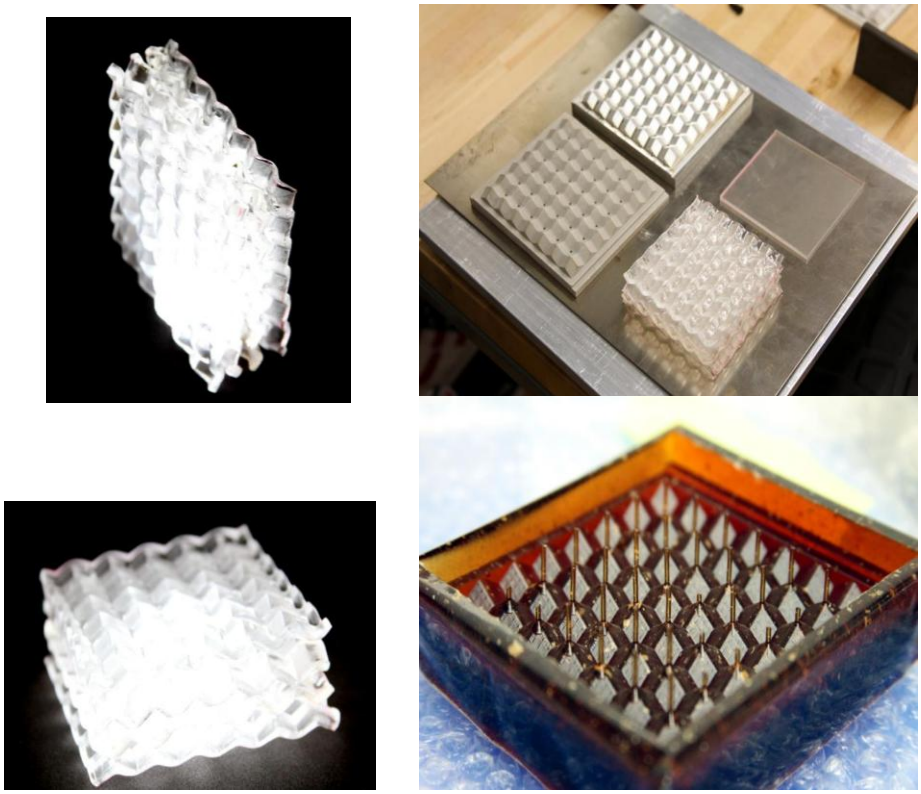

Figure 6. Tortuosity substrates produced with transparent acrylic waveguide sheets

Additionally, the corrugated acrylic surfaces were fabricated to create the sufficient gas interaction with large surface area of catalysts. The various components of the manufacturing process are illustrated in the **Figure 6**. In this approach, we create a model using computer controlled machining or 3D printing. We then create a mold of the model using a high temperature material. That mold is in turn used to make an aluminum cast. The aluminum cast is then heated, and with vacuum, the edge-lit material is shaped into a close approximation of the goal geometry, and serves as a test structure for optical measurements and catalyst deposition.

Flow Dynamics and Visualization

In order to better understand the mixing problem, we are proceeding with experiments that consider a finite set of geometric elements that compose the high tortuosity flow device. The hypothesis is that with characterization of flow behavior within each element, it will be possible to predict total mixing efficiency with a chain of such elements.

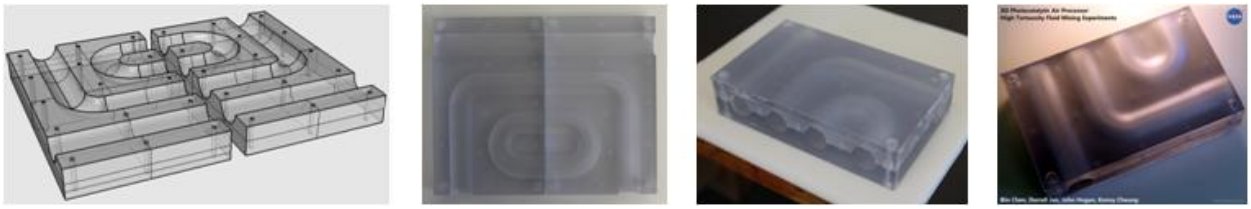

Figure 7. Modular mixing experimental device (L to R) CAD, top view, CNC milled polycarbonate, assembled

Considering various fabrication techniques, and the results from the flow experiments, we may pursue laminated pop-up designs such as origami interleaved tube cellular materials, which allow for adjustable volume ratios, maximal interfacial surface area, and production by lamination of flat sheets. Preliminary parts for testing flow visualization (NOT the actual tortuous flow paths yet) were machined by Cheung. The first picture shows one part (lower) that has been polished for optical clarity. The two parts together were sealed and a flow with a visualizing agent was introduced to check the flow visualization technique.

We performed preliminary flow visualizations (**Figure 8**) on relatively simple geometries. The third image from the left shows green particles suspended in water, flowing through a curved section which has a cross-section diameter of one inch. The bulk flow is a few cm/sec. Particles near the wall move very slowly or not at all, while the particles in the interior are

Figure 8. Far left: Machined flow channels. Left: Fluorescent particle synthesis. Right: Secondary flows visualized by green particles. Far Right: Newer fluorescent particles.

moving fast enough to leave streak paths, even in a single video frame. As expected, the streaks indicate velocity components in both the primary and tangential directions, showing secondary flows. There is some clumping of particles which will be addressed, by additional mixing and the addition of some surfactant. The cloudiness is due to less than perfect surface polishing, which is also easily addressed.

Pressure and diffusion characterizations for device modules were studied in analytical Hagen-Poiseulle modeling without extensive computing power. We have modeled device volume, reaction rate and input energy using an analytical solution to Hagen-Poiseuille equation to describe the laminar flow. We focused to understand the pressure drop when the reaction gas enters the tubular device channel:

$$\Delta P = \frac{8\mu LQ}{\pi r^4}$$

where μ is the viscosity, L is the length of the device channel, Q is the volumetric flow rate and r is the radius of the channel. By solving a second-order differential equation, we can generalize the conical configuration to series of straight channels of different radius. We end up with

$$\Delta P = \frac{\phi}{2\pi^2 \int_0^1 x\left(\int_0^x \frac{x^2}{f(x)}dx - \int_0^1 \frac{x^2}{f(x)}dx\right) dx}$$

to numerically evaluate the gas diffusion as it passes the tubular device channels**.** **Figure 9** shows that the diffusion length is linearly proportional to the flow concentrations with the radius of tubular reaction channel. This evaluation should be considered with the light transmission length when the device is assembled.

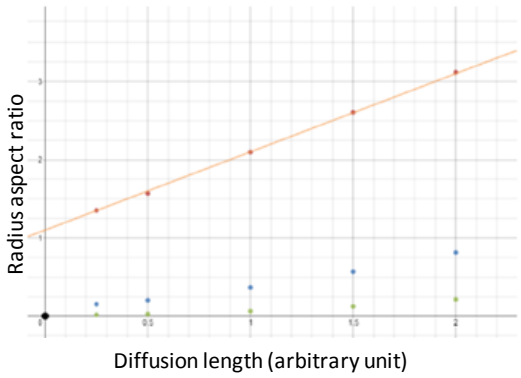

exp:1	2*r*	4*r*	6*r*	8*r*
0.25 cm	1.3519	0.1517	0.0170	0.0019
0.5 cm	1.5678	0.2025	0.0261	0.0033
1.0 cm	2.0967	0.3657	0.0637	0.0110
1.5 cm	2.6075	0.5673	0.1233	0.0266
2.0 cm	3.1175	0.8134	0.2131	0.0513

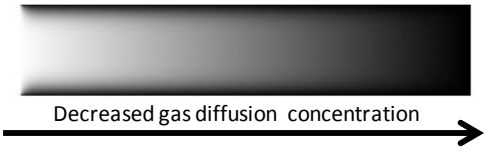

Figure 9. Numerical simulation of diffusion pressure drop in the tubular pathway

Experimentally, we 3D printed "Lego"-like pieces to test our model in order to extrapolate to scale-up more complex device configurations. Similarly, in the confined space of cabin or space station, transport systems become critical to as part of the life support of purifying waste gases,

liquids and solids. For example, **Figure 10** shows the reaction channel design we have recently developed for the fluid dynamic optimizations, to model ambient CO_2 flow catalytic reaction in a module reactor designed by our team. The "Lego"-like polymer reactor modules and sizes are configured together in straight or curved transport channels, depending on the mixing and transport requirements of the reactant gas. Our students have used the space shop at NASA Ames Research center to print all the 3D structural designs. We also studied different substrate materials (aluminum foil, polyethylene transparencies, and carbon paper) to deposit the novel catalysts developed using a piezoelectric nano-jet printer (Dimatix Fuji Film). The high surface area of fractal design would boost the photosynthesis conversion rate of CO_2 and water into methane and oxygen.

Figure 10. "Lego-like" 3D printed device module that can be individually designed and configured.

As the "Lego" configuration varies, we therefore allow the flow transport to change according to the tubular configurations of catalysts deposition, light illumination and product collection. For example, the length of reaction pathways and compositions of catalysts would affect the conversion efficiency, while the radius of the tubular structures also changes the CO_2 gas flow rate, diffusion length and finally light illumination. These similar parameters can be applied to stacked origami sheets and corrugated waveguide acrylic arrangements. **Figure 11** shows that the concentrations of reaction gas diffusion are proportional with the tubular tortuosity length and radius.

Optical power measurements and control

Work has progressed on the development of methods for conducting light from external sources into the photocatalytic reactor. The constraining design principles include minimizing the power required for light generation, ensuring that the most efficient wavelengths for catalysis are present, and uniform light distribution/intensity to catalyst surfaces. When combined with desired reactor properties, such as increasing the catalyst surface area per volume, uniform and low backpressure gas flow, and intermittent catalyst regeneration, the methods employed for delivering light become an integral part of the reactor form and function. Current methods

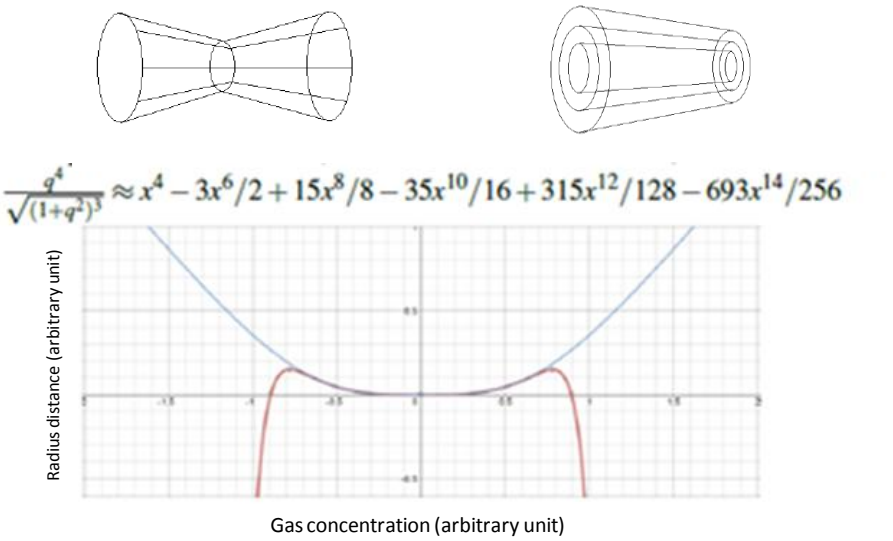

Figure 11. Hagen-Poiseuille modeling of gas concentration dependence on the radius of the diffusion pathway.

include the integration of optical channels within the reactor that conduct light from external concentrated sources for the selected catalysis reaction areas. Aside from employing a conventional optical fiber, we are examining the additive manufacturing of transparent pathways that are "printed" as light fibrils within the reactor structure to provide highly dispersed light directly onto the catalyst surfaces, and possibly from within the electrode itself. This can potentially allow a highly increased catalyst surface area density with minimal energy conductance loss.

The origami sheets are mechanically flexible and can be adapted to various configurations to allow the CO_2 gas flow to maintain the maximum interactions with the photo sources. In addition to evaluate the gas transport through optimizing device configurations, optical power distribution measurements helped the team to gain significant insight to the device design and light delivery.

Figure 12 shows the omni-light guided by the formation of the origami acrylic sheets inside a tubular and radiated over a planar origami surface. The surfaces serve as the catalysts substrates and form tortuous pathways as CO_2 gas flows through. More importantly, we can vary the flexible angles of the surfaces to control the overall light transmission and reflections. The optical power distributions on the acrylic waveguide substrates were studied with wavelength specific laser sources, as well as a 1:3 concentrated solar simulator with AM 0 (air mass) to model the space solar radiation. DPSS 532 nm and He:Ne 633 nm lasers are chosen to investigate the photo energy absorbed by catalysts and heat generated respectively. We used laser sources to correlate the optical power distribution and catalyst deposition at each energy range.

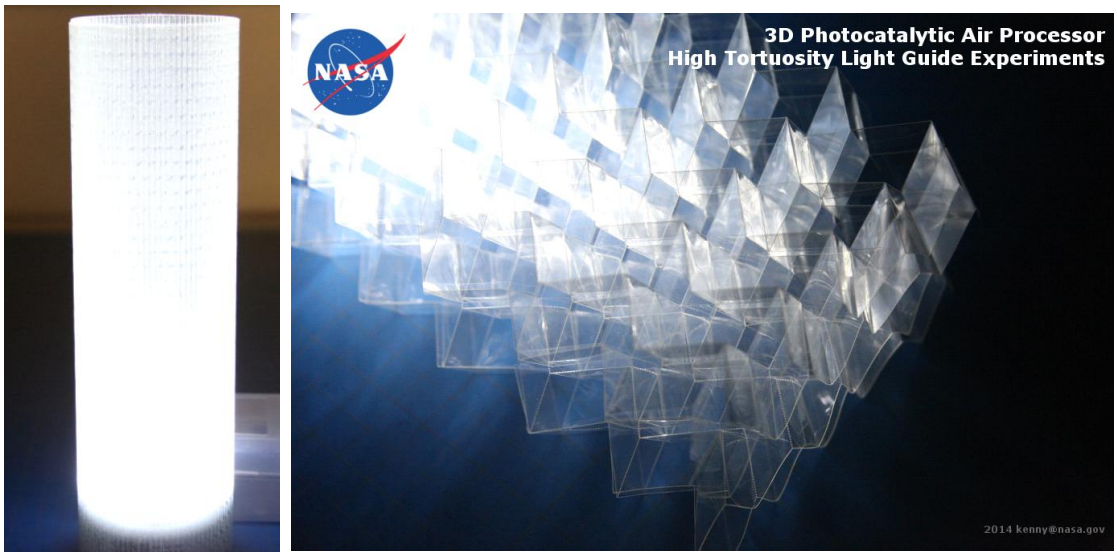

Figure 12. Examples of origami acrylic sheet configured to demonstrate the trapping and control of the photo energy with origami acrylic waveguide substrates in cylindrical (left) and flat (right) formations.

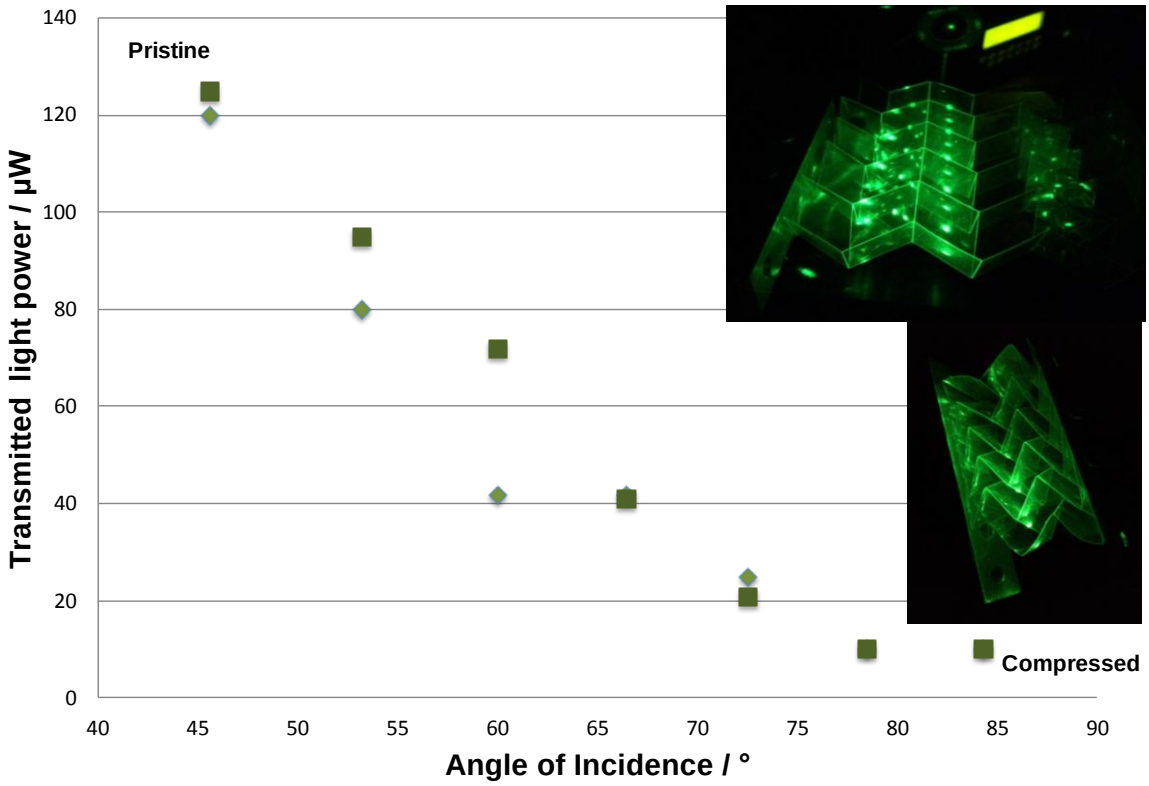

Figure 13. Optical power measurement of a 532 nm DPSS laser with 3.0 µw incident power.

The optical power distributions on the acrylic waveguide substrates were studied with wavelength specific laser sources, as well as a 1:3 concentrated solar simulator with AM 0 (air mass) to model the space solar radiation. DPSS 532 nm and He: Ne 633 nm lasers are chosen to investigate the photo energy absorbed by catalysts and heat generated respectively. We use laser sources to correlate the optical power distribution and catalyst deposition at each energy range.

For example, **Figure 13** shows an example of the wavelength specific experiments that demonstrates the optical power control and light dispersion by adjusting the shape of the single origami acrylic sheet. The transmitted power from the waveguide drastically decreased when the origami structures are compressed so the laser light passes the critical incident angle to all the coated planes. While we can vary the gas flow by compressing the origami sheet, we simultaneously adjust the light power distribution at reaction centers.

Figure 14 shows the similar power dependence when we test a series of acrylic sheets of variable thicknesses. While it is linearly proportional to the initial laser power, as the absorption increases with the thickness, the dependence of incidence angle become predominant for the transmission beyond the normal incidence angle (around 60º). Using the 3D printing manufacturing approach, it is possible to precisely design the light distribution by size, thickness and shapes and catalyst deposition in rows and columns in the origami structures.

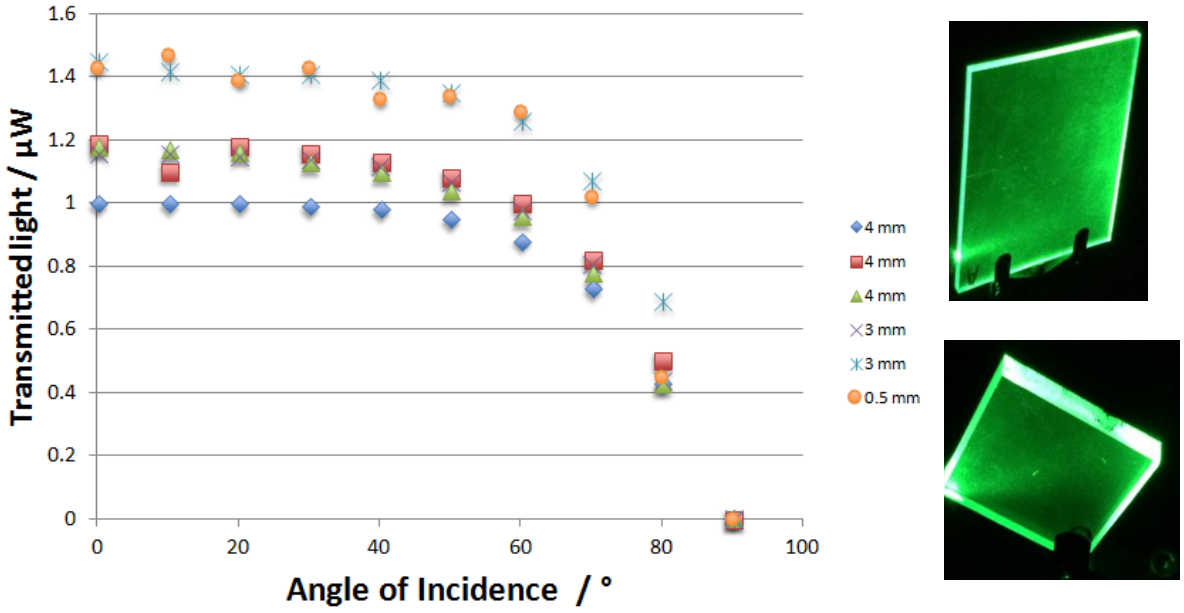

Figure 14. Transmitted power measurement from substrate light absorption and angle of incidence

2. Catalyst development and optimization

We have consistently demonstrated in Phase I studies the reproducibility and robustness of the catalyst materials synthesis and the characterization of materials structures and composition in

device fabrication and optimization platform. Cu/TiO_2 catalysts are reproduced and proved to be very stable under the ambient temperature and light conditions. In fact, the catalysts stored in aquatic solution since July 2014 has still been printed and tested well. Charged by the success, we did an extensive literature survey to investigate other potential catalyst candidates (summarized in **Table 1**). Since our device platform can be constructed using combinatorial chemistry of catalyst depositions, we will able to determine the catalyst candidates and optimize the selectivity and the conversion efficiency in systematic Phase II studies.

Table 1. Survey of catalyst studies: energy, starting materials and products

	Reductant	**light source**	
Pt/low-dimentionalTiO2 nanotubes (TO-NT), Pt/TiO2 nanoparticle P25 (TO-NP)	water vapor	300W Hg lamp (wavelength 365nm)	
TiO2	water	200 W Hg/Xe-lamp	
2.0 wt% Pd/TiO2 sol gel	water	350 W Hg lamp	
TiO2 particles	water	8W Hg lamp	
Nafion layer over Pd-TiO2	water		
0.5%Cu/TiO2-SiO2	water vapor	A Xe lamp, 250 nmolo400 nm, 2.4 mW/cm2	
TiO2 nanotubes	water vapor	100W Hg lamp	
Pt/TiO2 nanotubes	hydrogen		
CdSe/Pt/TiO2	water	300W Xe arc lamp wavelength>420nm	
TiO2 particles	Aqueous NaHCO3	15W 365nm	
TiO2 with different concentrations of 2- propanol	water	350nm light	TiO2 anatase, -325 mesh
TiO2 nanotubes with different annealing temperatures	water vapor		
Ag/TiO2	water	UV 8W Hg lamp 254nm	
Rh/TiO2	hydrogen	Hg lamp wavelength=280nm,370nm,450nm	
Cu(0.25 wt%)-Fe(.025 wt%)/TiO2 films	water vapor	150W UVA lamp UVA(320-500nm), UVC(250-450nm)	Cu(0.5 wt%)-Fe(.05 wt%)/TiO2/optic fiber 0.91
Ag/TiO2	0.2M NaOH solution	UV 8W Hg lamps 2554nm	
Cu/TiO2	water	8W UVA	
Pt/TiO2	water vapor	150W UVA Lamp, 75W daylight lamp	
N3 dye Cu(0.5 wt%)-Fe(0.5 wt%)/TiO2/optical fiber	water vapor	150W high presure Hg lamp	
same as 74			
Pt loaded ex-Ti-oxide/Y-zeolite	water	75W lamp, wavelength>280nm	
Ti-ß zeolites			
Ti-Ps(h, 50)	water vapor	100W high-pressure Hg lamp	
same as 74			
Ru/TiO2	water	1000W Hg lamp 365nm	
TiO2 film	water		
TIO2 pellets	water vapor		
kaolinite/TiO2	water	8W Hg lamp	

The conventional photoelectrochemical reaction would involve multistep reactions shown in **Figure 15** at the surface of metal electrodes in solution. The fundamental advantage to use composite catalysts is that all reaction steps occur in the submicron scales and can be controlled by carefully designing composite catalysts with the electronic and microscopic structures at the reaction surfaces. In addition, not having the reaction in the aquatic media not only reduces the hardware complexity, volume and weight, it naturally eliminates excess protons that could drive many other endothermic reactions, thus increasing the reaction selectivity.

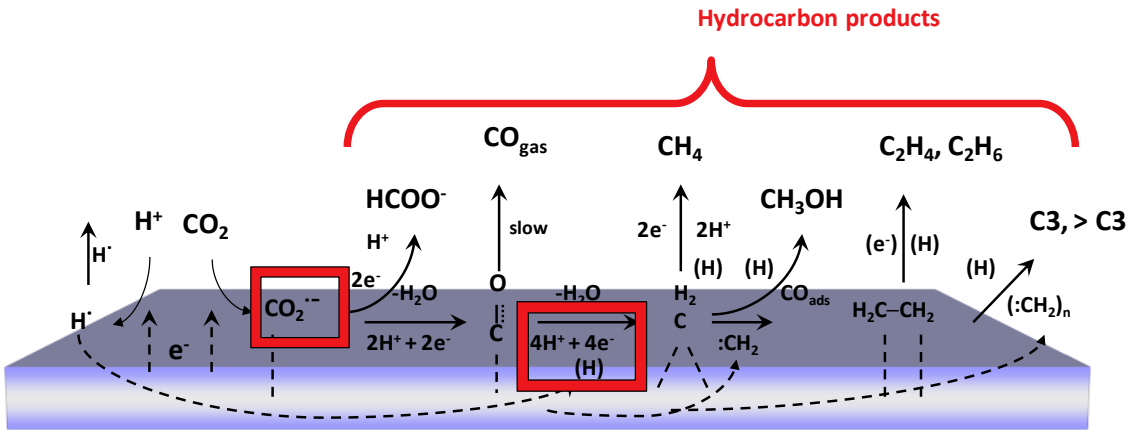

Figure 15 Multistep catalysis conversion of CO_2 absorbed on the transition metal catalyst surfaces. The products can be tailored by catalyst selectivity according to mission needs. (centi, 2007)

In addition, Ni/TiO_2 composite catalysts are under development for higher carbon chain hydrocarbon species. Our preliminary studies confirmed the proposed candidates nickel catalysts (shown in TEM images in **Figure 16**) for the conversion of the hydrocarbon species.

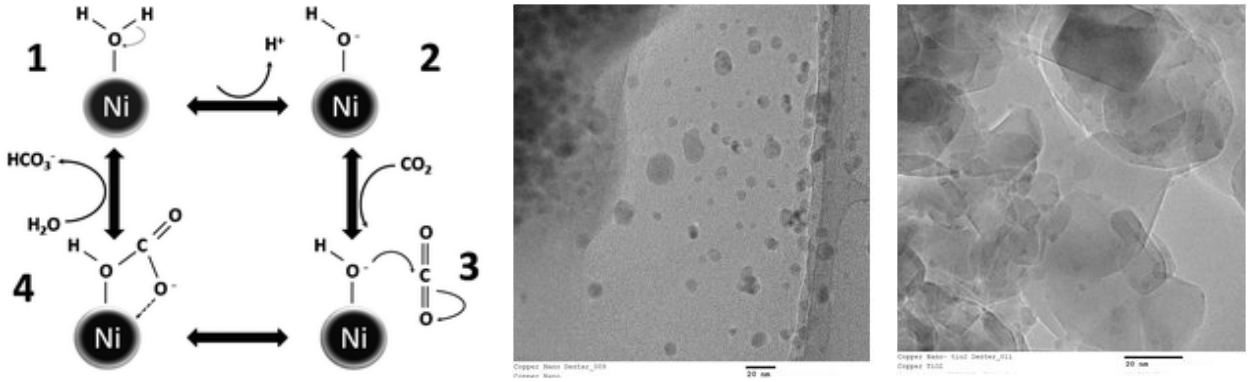

Figure 16 The catalytic pathway of CO_2 conversion on the surface of nickel nanoparticles 2 to 10 nm shown in transmission electron microscopy (TEM)

Table 2 summarizes our studies of the characteristics of both Cu and Ni TiO_2 composite catalysts, which warrant further studies in Phase II. We now have two excellent catalysts candidates for phase II optimization. Nickel catalyst was determined to be the alternative choice for the following reasons: 1) potential high yield of longer chain hydrocarbon and condensed phase product, 2) easy recovery due to its magnetic properties, 3) non-toxic and easy handling process. The condensed phase of predominant resultant product is carbonic acid, which can easily be mineralized to environmentally friendly solid minerals including magnesium carbonate, calcium carbonate and dolomite, which could be used a building material.

Table 2 Comparison result of hydrocarbon conversion catalysts

	Cu/TiO_2	**Ni/TiO_2**
Synthesis and growth control	facile	facile
Deposition and substrate coating	Plasma printing thin film deposition	3D printing (task in Phase II) thin film deposition
Materials stability	stable	stable
Main products	CH_4 (fuel), ethylene (minor)	carbonic acid (mineral precursor), ethylene
Main detection methods	GC	Raman , XPS, NEXAFS
Energy Efficiency	10%	Task in phase II

Catalyst deposition and coating

Three thin film deposition techniques shown in **Figure 17** have been used at NASA Ames Research Center. Langmuir Blodgett set up (left) is a layer by layer deposition technique that we use for monolayer deposition for the small substrates. The nano-jet Dimatix printer (middle) also has the potential to play a major role in the manufacturing catalyst deposition process. Langmuir Blodgett monolayer, plasma and nano-jet printing allow us to have complementary processes for 3D device prototype design.

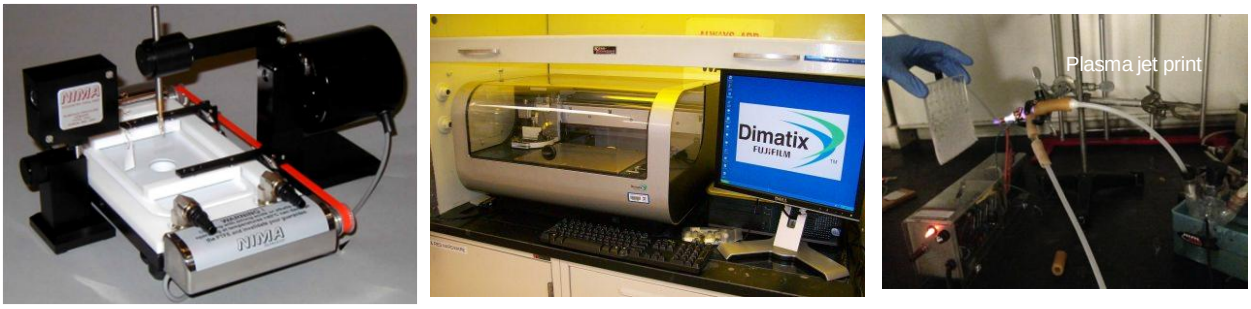

Figure 17. Thin film deposition experiment set ups at ARC labs from left to right: Langmuir Blodgett monolayer deposition trough, piezoelectric nano-jet printer (Dimatix) and a home-*made* plasma jet printing

The preliminary studies show the best results by using the aerosol combined atmospheric pressure (ACAP) plasma printing for any single fabrication involves a) plasma pre-treatment to increase adhesion b) highly uniform and enhanced deposition of nanostructures on the substrate and c) post-plasma treatment to remove moisture. In addition to these features, the ACAP plasma printing could be used to deposit multiple components like conductive traces, semiconductor materials, dielectric coatings to fabricate electronic devices in a single tool. Surface compatibility posts the challenge to dispense and control the catalysts. Fortunately, both Cu and Ni TiO_2 co-catalysts are easy media to deposit with the thin film deposition

techniques of Langmuir Blodgett and plasma jet printing. A 3D model (**Figure 18**) of the atmospheric plasma print head is comprised of (1) a concentric quartz spray nebulizer (2) the spray chamber complete with a drain located at the base and (3) the spray nozzle which is equipped with two copper electrodes spaced approximately 3cm apart. There is also an additional gas input line for introducing more gas species to facilitate ignition as well as focus the spot size. Ink is pumped into the nebulizer via a syringe pump. Concurrently, helium gas is also flown into the nebulizer via a gas input line. As the ink reaches the tip of the capillary line, it is bombarded by the rapid gas flow and a fine mist is formed in the spray chamber. As the mist condenses on the sidewalls of the spray chamber, larger droplets will fall into the drain. The finer aerosol particles will have enough momentum to reach the electrode junction. They are shielded from ignition by the inner Pyrex tube of the print head. The additional gas inlet is ignited and accelerated through the nozzle of the print head. The heavier droplets will accumulate over the drain of the spray chamber until the negative pressure at the end of the capillary line of the drain sucks the excess ink out. This ink can be recovered by collecting it in a container.

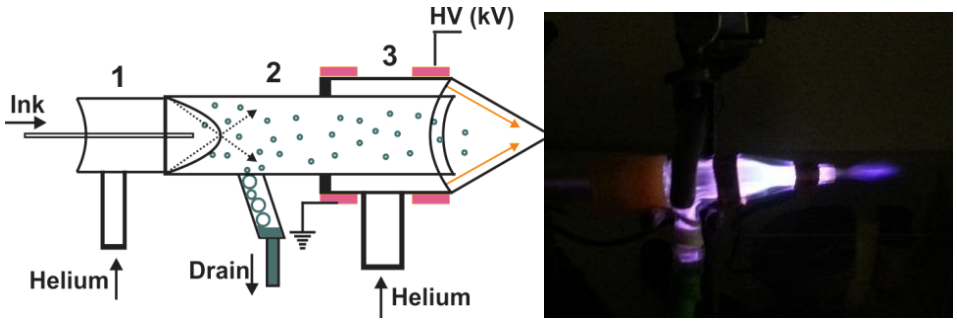

Figure 18. a) Schematic of atmospheric pressure plasma printer. b) photograph of plasma extending from the pipet printer head

The Cu/TiO_2 catalyst solutions have been formulated to obtain homogenous depositions onto a range of substrates including silicon, acrylic and metal surfaces. To scale up the formulation, we employed a stable, well-adhered and repeatable deposition by ACAP plasma-based printing. The ACAP plasma printing performs multiple functions in a single tool with superior deposition capabilities. As it is cold atmospheric plasma with a dielectric barrier, the current associated is extremely small (i.e., milliamps). Hence the plasma causes minimal or no thermal effect on the substrates. The aerosolized ink is now introduced to the high energy plasma jet and accelerated out of the nozzle to a relatively fine spot size. The spot size can be altered by altering the print head nozzle diameter. The microscopic images (SEM) demonstrate the controllable, homogeneous depositions shown in **Figure 19.** The conventional drop cast and spin coating relies on the sheer cast force and viscosity of the materials to control the dispersion and often result overlay and clusters in the film formation.

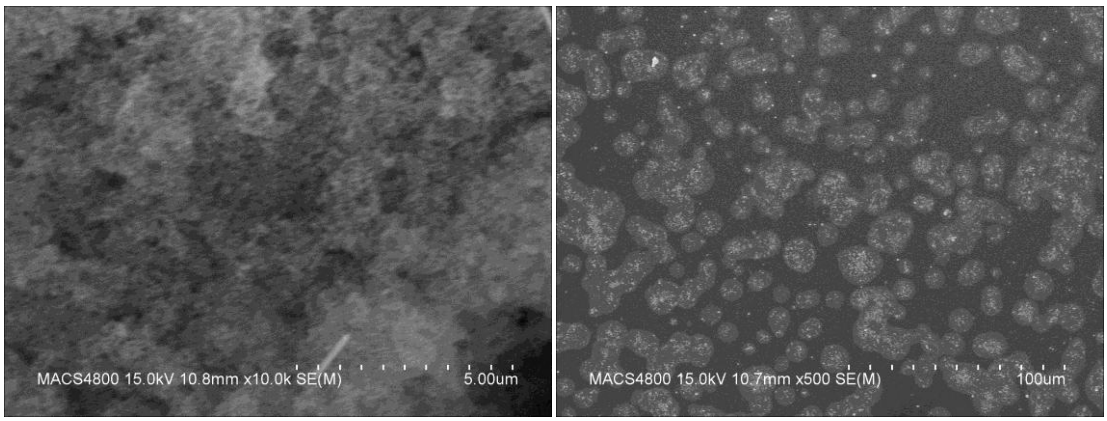

Figure 19. Scanning electron microscopy (SEM) images showing controlled homogenous film produced with plasma jet printing (right) in comparison with conventional casting (left)

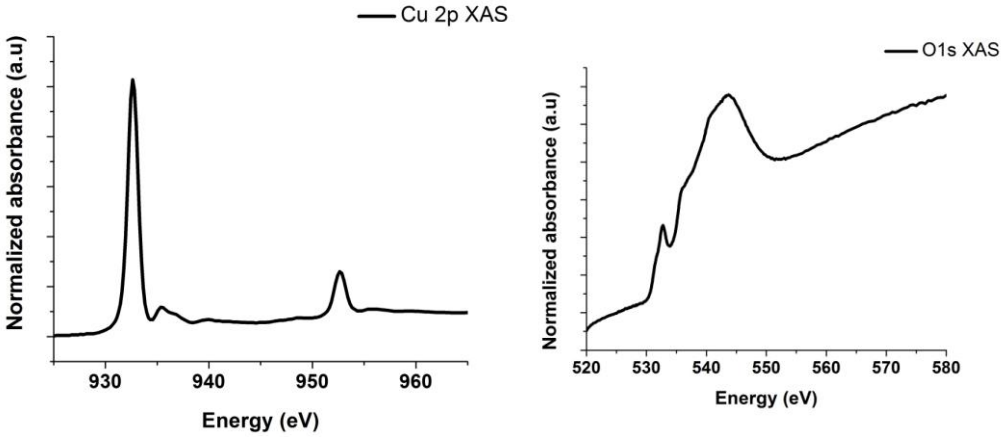

Figure 20. Copper L edge X ray absorption spectrum of copper oxide nanoparticles deposited by plasma printing.

Near edge X ray absorption spectroscopy (NEXAFS) is a high sensitive element and composition characterization technique. **Figure 20** shows high purity of Cu composition after extended storage time with low presence of oxide in plasma printing Cu nanoparticle films. The spectrum confirms the presence of low concentration of copper in oxidation state +2.

The advancements of printed liquid and solid catalytic materials also led us to explore the biologically-inspired fractal design of an "artificial tree" that can enhance HTPEC photosynthetic performance. We have looked into whether multi-scale algorithms would guide a design of and manufacturing these devices. Natural transport systems such as

Figure 20. Fractal patterns in retinal blood vessels and tree branches.

blood vessels, tree branches, and roots often have fractal patterns in order to maximize their effectiveness in a tightly contained space (**Figure 20**). Fractals have the advantage of a high surface area. The high transport efficiency of volume of blood in the human body, or the nutrients in a tree, is known to transport in an optimal, volume-efficient package. A fractal with a fixed volume theoretically has an infinite surface area. Therefore, in practice, the surface area of a fractal is limited only by manufacturing capabilities: the features of the materials compositions, and more importantly, the manufacturing ability and precision control of fine assembly details.

Maximizing surface area in the confined volume can be illustrated by how Koch snowflake fractals are generated (**Figure 21**): 1) Start an equilateral triangle. 2) Attach an equilateral triangle with length equal to one-third of the original side length of the polygon currently on the paper to the middle of every side. 3) Repeat step 2 infinitely to obtain the printing/deposition feature size. Step 2 clearly increases the side length of the shape by a factor of 4/3, so hence the Koch fractal has infinite side length and the side length after iteration n is $\left(\frac{4}{3}\right)^n$ times the original side length. For example, if a manufacturing process could carve out sides as fine as .5 microns and the catalyst was based on a triangle 1 cm in length, then since $\log_3 20000 = 9$, 9 iterations could be made. This would result in a side length of $\left(\frac{4}{3}\right)^9 = 13.3$ times that of the original triangle. Building a prism with the Koch Snowflake as its base extends this example to three dimensions. Once a mathematical design is set for a fixed volume, a fractal model will yield the highest surface area at the orders of magnitude increase in the interaction pathways, and be ready with digital precision for 3D printing technology.

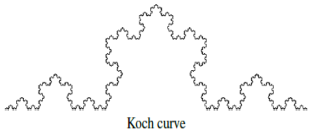

Figure 21. Example of fractal pattern Koch snowflake

System design and integration analysis:

A preliminary systems analysis was conducted to guide future designs of the photo-catalytic CO_2 conversion hardware. As a first step, the major parameters involved in the overall design were identified and schematically represented (see Figure 22). The three main categories were divided into the management of the process inputs, the processor itself and the process outputs. The "Systems Resources" box in the lower right corner involves the impact to flight.

We have started assembling data for making a comparison between existing NASA CO_2 removal technology and our approach. In other cases, we will make some mass and volume estimates based on publicly available information of ISS hardware. This should be sufficiently accurate for a preliminary comparison. Additionally, work has begun on developing the overall process strategy required for application in spacecraft. This includes examining whether the system should use nominal cabin air or a concentrated CO_2 stream, humidity management for optimizing the O_2 and proton production, and the separation of the product gases for eventual use or venting. This analysis is critical for determining the full complement of components required for successful integration and operation.

Considerably more physical development of the hardware is necessary to be able to accurately quantify many of the parameters. Regardless, the initial analyses have led to a down-selection of system design and integration decisions. For example, examining the process of downstream management of the process gaseous outputs has led to the decision that the overall reactor configuration must be an enclosed approach, as opposed to exposing open surfaces to the cabin air for a "flow-over" approach. This is because the process by-products will include significant amounts of CH_4 and H_2 which would pose potential risks to safety if they were released to the general cabin air. Additionally, the ability to control the stoichiometric ratio of CO_2 and H_2O is lost unless there is a contained reaction volume, with discreet control over inputs. This is a critical aspect to regulate that amount of O_2 production. In general, the amount of water vapor contained in spacecraft air will be several times higher than the stoichiometric requirement with respect to the amount of CO_2 present. Without optimizing this ratio, the reactor would likely split more water than necessary to supply the O_2 for the crew. Therefore there is a need to control the amount of water electrolyzed to match the CO_2 reduction reactant (H_2) requirement.

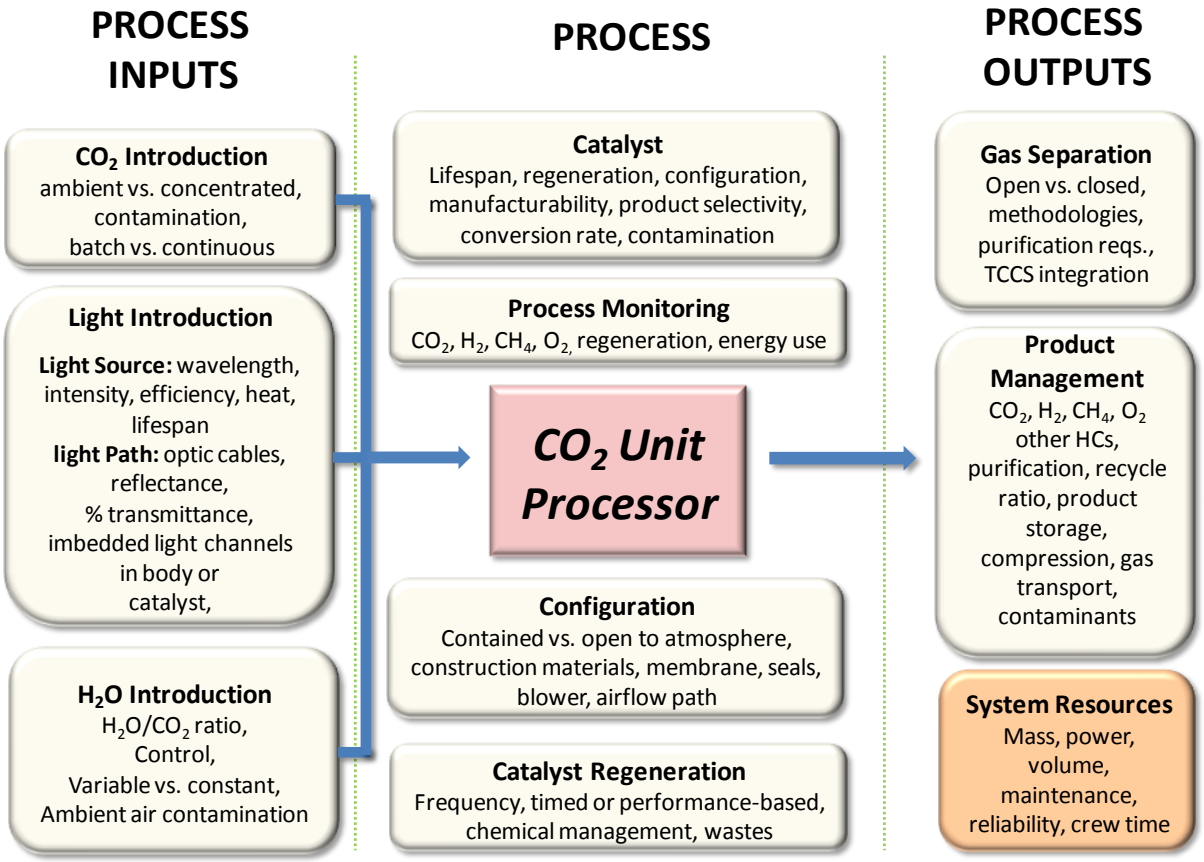

Figure 22. Overall parameter schematic for the systems analysis of the HTPEC CO_2 conversion hardware development process.

This need to optimize the ratio of CO_2 to H_2O requires dynamic control for effective process performance. As H_2O is in stoichiometric excess under nominal conditions, it is necessary to either decrease the amount of H_2O present in the air via removal, or to selectively concentrate CO_2. As both the humidity and CO_2 concentrations vary with time, these processes would require dynamic controlled. Therefore, if the air were dried to decrease, but not eliminate, the amount of water vapor present, it would need to dynamically match variable CO_2 concentrations. Cabin atmosphere CO_2 concentrations will vary based upon the number of crew present, CO_2 removal performance, and the level of crew metabolic activity.

Figure 23 displays two major pathways for HTPEC integration for human life support. Variant A depicts an integration scenario that employs a tunable air drying system that allows a variable outlet relative humidity to match CO_2 concentrations. There are several means to design this system, perhaps the most straightforward being the use of a regenerable drying bed (e.g., silica gel) that thoroughly removes water from a portion of the inlet air and allowing a regulated amount of air to by-pass the dryer. Another approach could be the use of low-power, passive membrane dryers that could use the overall process air to pre-dry the inlet air. This approach is plausible because HPTEC system converts the incoming water vapor to H_2 and O_2, thereby effectively "drying" the outlet airstream. If the HPTEC was designed to nearly fully react all inlet H_2O, it would become a very effective air drying system. Proper control of the system would require both CO_2 and H_2O vapor sensors.

Product gas separation will also be an important design consideration. Inlet gases to the system will likely include O_2, N_2, CO_2, and H_2O vapor. Inside the HTPEC reactor, H_2, methane and/or ethylene (or other target hydrocarbons) and potentially small amounts of other contaminants will also be present. Gas separation processes will need to be able to recover the O_2 and N_2 to return to the cabin, as well as partition the target hydrocarbons for use (e.g., propellant or feedstock molecules) or discharge via venting. Other process products that are considered contaminants would be conducted directly to the spacecraft trace contaminant control system for treatment.

The overall performance of the system will be a function of a wide range of factors. Of critical importance will be the selectivity of the catalyst for making the target hydrocarbons, as well as its longevity and capacity for regeneration. The reaction system will need to be designed to have near-complete treatment of the CO_2, as well as thorough depletion of the reactant hydrogen. This involves designing the HTPEC reactor to cease the splitting of water prior to the outlet so as to avoid H_2 release due to inadequate opportunity for uptake and conversion. This can be accomplished by either changing the catalyst in the end reaches of the flow path or by not exposing this area to light. Additionally, reliable and feasible regeneration techniques will be required to periodically restore maximal catalyst performance. A fundamental method to address this issue is to select catalysts that resist product coating. These are often more stable metals such as gold. Other methods under consideration use the washing of surfaces with neutralizing agents.

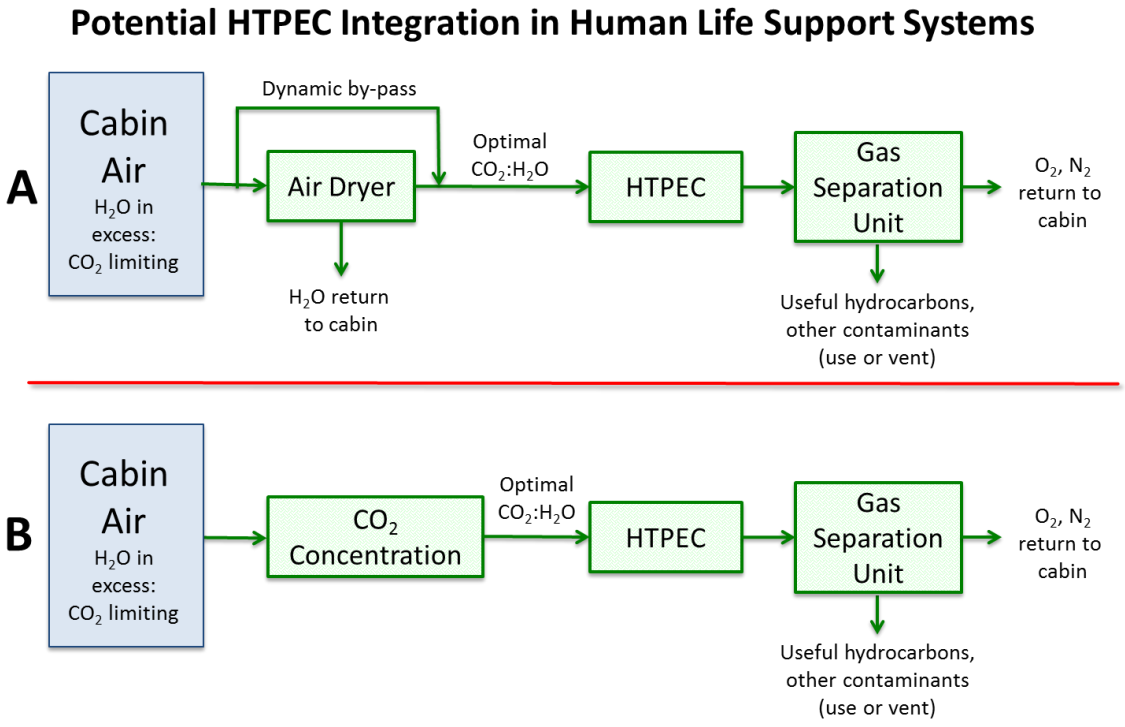

Figure 23 Two potential methods of HTPEC integration for human life support systems. Variant A (top) depicts the simple method of dynamically controllable air drying to attain optimal CO_2:H_2O reactant ratios. Variant B displays a method using CO2 concentration instead of drying. This option

Alternatively, variant B in **Figure 23** depicts the approach of concentrating the inlet CO_2 to match the varying relative humidity. CO_2 concentration would not require bringing the product air to pure CO_2, such as is the case for CDRA. Instead, CO_2 concentration would only be required to meet stoichiometric requirements. More complete CO_2 concentration could also be utilized (including pure CO_2). Despite the need increased processing, the total amount of gas flow requiring treatment in the HTPEC could be greatly decreased. This would result in much smaller HPTEC mass, volume and power.

Another potential use for HTPEC is in ISRU applications, particularly for use in Martian surface missions (see **Figure 24**). Because the atmosphere is nearly 96% CO_2, it is likely possible to directly use the atmosphere with added water vapor (also potentially from ISRU sources) to generate O_2 and targeted hydrocarbons for propulsion, life support, etc. This application is likely easier to implement as compared to human habitation systems in that creating optimal reactant ratios would be simplified, and final product gas separations would be facilitated.

It is apparent that a number of different methods are possible for operation of the HTPEC. Future analyses require obtaining additional data from physical trials, including stoichiometric data

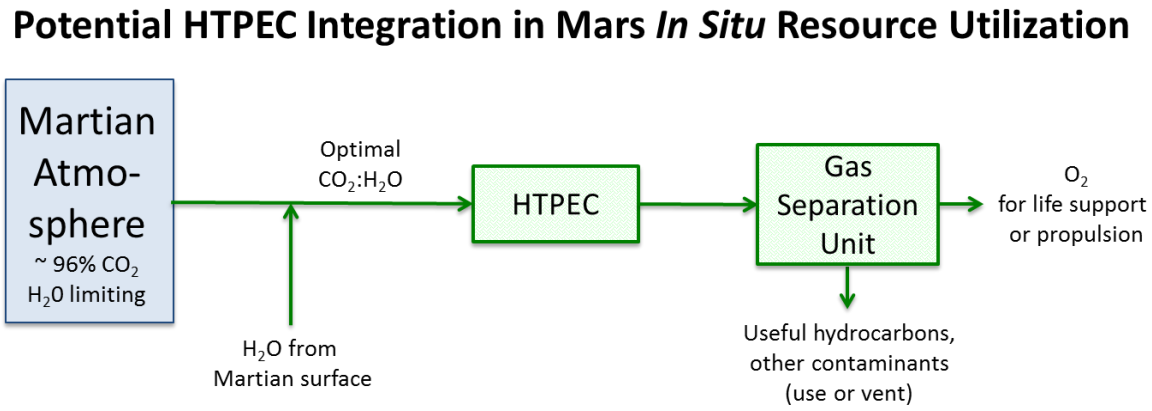

Figure 24. A potential configuration of HTPEC for use in *In Situ* Resource Utilization operations.

regarding acceptable/optimal CO_2 to H_2O ratios, catalyst regeneration methods and resources required, light input (wavelengths/intensity) requirements, gas separation techniques and performance, and general mass/power/volume data to support an equivalent system mass (ESM) analysis. It is anticipated that future work will employ parallel analysis and hardware development efforts to maximize the potential for application and cost effective design.

Using data from previous experiments, we performed a first order estimate of the surface areas needed to demonstrate the acrylic substrates. From our preliminary CO_2 conversion results of 1000 microliters of CO_2/mg catalyst-hour and using 1 g of catalyst coating over 100 meters^2 by our average surface analysis (BET), we obtain $10^{\wedge-2}$ liters of CO_2 per square meter per hour. Given the average crew member CO_2 production is 1kg/day, at 44 g/mole, and 22.4 liters/mole, this is 500 liters per day, or about 20 liters/hour. 20 liters/hour divided by 10^{-2} liters CO_2/sq meter/hour means we need 2000 square meters.
Using the information from
http://www.nasa.gov/mission_pages/station/research/experiments/608.html

Eight of the EXPRESS Rack positions are the size of a shuttle Middeck Locker with a carrying capacity of 72 lbs and an internal volume of 2 ft³. The remaining 2 positions are International Subrack Interface Standard (ISIS) drawers, which has a carrying capacity of 44 lbs and an internal volume of 1.3 ft³. The total volume = 8*2 + 2 * 1.3 = 18.6 cubic feet. = 0.527 cubic meters, or 527 liters. 2000 or even 4000 sq meters seems plausible, with thin reactor walls. The catalyst would be coated at about a micrometer depth (to provide increased surface area) to accommodate 6 crew in the same single rack volume. The additional surface area allowed by fractals (at least 10 to 100 times) should do this easily. So we have believed that only a half rack of the two units currently used on ISS is needed with our technology (illustrated in **Figure 25).**

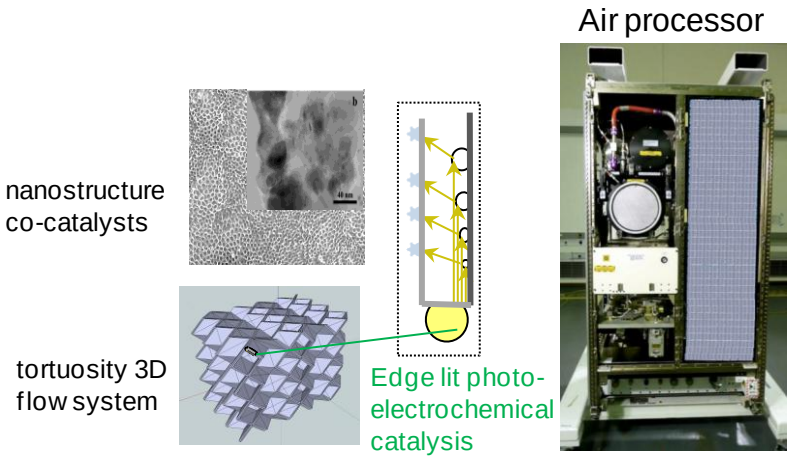

Figure 25. Half of the ISS rack volume is needed for the proposed approach.

Administrative summary:

Despite the significant delay due to procurement funding placement at NASA Ames, the team has progressed significantly in every proposed research area. The Phase I studies have attracted significant interests from Silicon Valley industrials from research pioneer Palo Alto Research Center, (PARC), to equipment manufacture Applied Materials Inc, optical engineering company CRI, to a start-up company are all onboard with our work at the different levels in market and technology advancement, ranging from the 3D printing materials to the artificial photosynthesis approach. Among them, we have identified the collaboration area with PARC and CRI and involved them in the Phase II proposal. We also involved a student from University of Chicago to study the economics of CO_2 manufacturing. We have contacted Wayne Gellett of eSonic in Menlo Park, we will stay in touch for their technology development which can enhance our research.

The team laid the solid ground work going forward for Phase II on the alternative catalysts and device design through system analysis and evaluation. We achieved all Phase I objectives to demonstrate the fundamental approach to convert useful hydrocarbon fuels with low pressure CO_2 atmosphere. We have applied novel materials developed *in house* using facile, space applicable synthesis methods. In addition, two new directions in optical and catalyst deposition are identified and studied for future integration. The project milestones and deliverables previously reported are summarized in the table below.

Task Plan	Proposed Schedule	Progress	Plan
A. Demonstrate the production and tunability of extrude-able catalytic polymers	Month 1-3	A number of catalyst materials are identified and prepared, they will be evaluated as the photocatalysis components.	Key photocatalyst and electrocatalyst nanostrucures will be optimized in Month 3

B. Demonstrate design and prototype of HTPEC device with active materials	Month 2-6	3D device power and thin film catalysts are modified for the set up	Gas conversion microreactor in three platforms will begin operating in Month 4
C. Determine optimal system integration and conduct trade studies	Month 2-10	Concluding to be a closed device and system design	Focus on efficient light delivery and mass transport design
D. Conversion test and optimization under ambient pressure and temperature	Month 6-9	The ambient pressure can be increased with a low voltage fan or an existing device	Delayed in responding the original scheduled timeline
E. Overall device optimization and development of Phase II research plan	Month 6-9	Optical studies and system designs for catalyst substrates	No change to original scheduled progress On time

Financial report

1	**FIRM NAME:**	NASA Ames Research Center
2	**FIRM ADDRESS:**	Moffett Field, CA
3	**LOCATION:**	(Same as 2)
4	**PROPOSAL TITLE:**	3D PHOTOCATALYTIC AIR PROCESSOR FOR DRAMATIC REDUCTION OF LIFE SUPPORT MASS AND COMPLEXITY
5	**TOTAL AWARD**	$100,000

Related Publications in the funding period:

Resultant patent application:
1. B. Chen, D. Jan, J. Hogan and K. Cheung, NASA Ames Invention Disclosure, and pending US patent application ARC-17371-1 "A Versatile Three Dimensional Printing Approach", 2014

Published patent:
B. Chen, J. Lake, M. Meyyappan, “Graphene Based Supercapacitor”, US 8940145 B1.

Peer reviewed publication
Cheung, K. C., Tachi, T., Calisch, S., & Miura, K. (2014). “Origami Interleaved Tube Cellular Materials.” Smart Materials and Structures, 23(9), 094012.

R.P. Gandhiraman, D. Nordlund, C. Javier, J.E. Koehne, B. Chen, M. Meyyappan, "X-ray Absorption Study of Graphene Oxide and Transition Metal Oxide Nanocomposites", J. Phys. Chem. C., 118 (32), pp 18706–18712 (2014)

Gandhiraman, R.P.; Jayan, V., Han, J-W., Chen, B., Koehne, J., Meyyappan, M. " Plasma Jet Printing of Electronic Materials on Flexible and Non-Conformal Objects", ACS Applied Materials and Interfaces. 3,12, p. 4640 (2014).

Conference paper in the related work

T.-M.J. Richardson, D. Jan, J. Hogan, R. Bohrer and D.K. Marson. Submitted. "Carbon Dioxide compression, storage, and delivery trade assessment", 45th International Conference on Environmental Systems, Technical Paper ICES-2015-064, Bellevue, WA, 2015

Darrell Jan, John Hogan, Gary Palmer, and Brian Koss. Submitted, "Progress on the CO_2 removal and compression system", 45th International Conference on Environmental Systems, Technical paper ICES-2015-064, Bellevue, WA, 2015

References

1. Ballard Fuel cell, http://www.ieee.ca/millennium/ballard/ballard_info.html accessed 12/10/13, and a microbial electrode from our own group.

2. Boxun H., Guild C., Suib, S. L., "Thermal, electrochemical, and photochemical conversion of $CO_2$to fuels and value-added products**",** *Journal of CO_2 Utilization*, 1, 18 (2013)

3. Bin Chen, Nicolas Londono, "Solar Powered CO_2 Conversion", pending US patent, 2013.

4. Bin Chen, "Synthetic biology pathways of artificial photosynthesis", Materials Research Society annual meeting, Boston. November 27, 2012.

5. Kenneth C. Cheung, Erik D. Demaine, Jonathan R. Bachrach, and Saul Griffith, "Programmable Assembly With Universally Foldable Strings (Moteins)," *IEEE Transactions on Robotics*, vol. 27(4), 718-729 (2011).

6. Cheung, K., Tachi, T., Calisch, S., Miura, K., "Origami Woven Tube Cellular Materials", pending review, 2014

7. Gabriele Centi, Siglinda Perathoner, Gauthier Winè and Miriam Gangeri 2007, *Green Chemistry,"* Electrocatalytic conversion of CO_2 to long carbon-chain hydrocarbons", **9**, 671-678

8. Gabriel Centi, Elsie Alessandra Auadrelli, Siglinda Perathoner, 2013, "Catalysis for CO_2 conversion: a key technology for rapid introduction of renewable energy in the value chain of chemical industries", *Energy & Environmental Science*, issue 6, 1711

9. R.P. Gandhiraman, D. Nordlund, C. Javier, J.E. Koehne, B. Chen, M. Meyyappan, 2014, "X-ray Absorption Study of Graphene Oxide and Transition Metal Oxide Nanocomposites", J. Phys. Chem. C., 118 (32), pp 18706–18712

10.

11. Gandhiraman, R.P.; Jayan, V., Han, J-W., Chen, B., Koehne, J., Meyyappan, 2014, M. " Plasma Jet Printing of Electronic Materials on Flexible and Non-Conformal Objects", ACS Applied Materials and Interfaces. 3,12, p. 4640.

12. Gattrell, M.; Gupta, N.; Co, A., "A review of the aqueous electrochemical reduction of CO_2 to

hydrocarbons at copper"**,** *Journal of Electroanalytical Chemistry*, 594, 1(2006).

13. Elysse N. Grossi, Aaron J. Berliner, John Cumbers, Hiromi Kagawa, Beeta Modarressi, John A. Hogan, Michael T. Flynn, "Potential Applications for Bioelectrochemical Systems for Space Exploration," 43rd International Conference on Environmental Systems, July 2013, Vail, Colorado, AIAA 2013-3331.

14. John Hogan, Bernadette Luna, Brian Koss, Gary Palmer, Paul Linggi, Zhe Lu, "The Low-Power CO_2 Removal and Compression System: Design Advances and Development Status," 42nd International Conference on Environmental Systems, July 2012, San Diego, California, AIAA 2012-3587.

15. Ito, K., Ikeda, S., Yoshida, M., Ohta, S., Lida, T., "On the reduction products of carbon dioxide at a p-type gallium phosphide photocathode in aqueous electrolytes", *Bulletin of the Chemical Society of Japan*, *57*, 583 (1984).

16. Nicolas J. Londono, Qibing Pei, Bin Chen, "Tandem Photoelectrochemical Laminar Flow Cell for Carbon Dioxide Reduction", The Society for Solid State and Electrochemical Science and Technology Meeting, Seattle, WA. June, 2012.

17. Julian Minuzzo, Thomas LaTempa, Nicolas Londono and Bin Chen, "Composite catalysts for photoelectrochemical conversion of CO_2", submitted to Nanolett, 2013.

18. Monnier, A.; Augustynski, J.; Stalder, C. "On the electrolytic reduction of carbon dioxide at TiO_2 and TiO_2-Ru Cathodes"**,** *Journal of Electroanalytical Chemistry*, *112*, 383 (1980).

19. Monsi Roman, Jay Perry, Darrell Jan, "Design, Development, Test, and Evaluation of Atmosphere Revitalization and Environmental Monitoring Systems for Long Duration Missions," AIAA Space 2012 Conference and Exposition, September 2012, Pasadena, California, AIAA 2012-5210.

20. Monsi Roman, Jay Perry, Darrell Jan, "Design, Development, Test, and Evaluation of Atmosphere Revitalization and Environmental Monitoring Systems for Long Duration Missions," AIAA Space 2012 Conference and Exposition, September 2012, Pasadena, California, AIAA 2012-5210.

21. Michael Nosonovsky and Bharat Bhushan (eds), "Lotus versus Rose: Biomimetic Surface Effects", Green Tribology, Green Energy and Technology, Springer-Verlag, 25, 2012

22. Perry, J.L, Abney, M.B., Knox, J.C., Parrish, K.J., Roman, M.C. and Jan, D.L. 2012. Integrated Atmosphere Resource Recovery and Environmental Monitoring Technology Demonstration for Deep Space Exploration. 42nd International Conference on Environmental Systems. AIAA technical paper 2012-3585

23. Rohsenow and Choi, Heat, Mass, and Momentum Transfer, Prentice-Hall, 1961.

24. Saladin, F., Alxneit, I. "Temperature dependence of the photochemical reduction of CO_2in the

presence of H_2Oat the solid/gas interface of TiO_2", *J. of the Chem. Soc.-Faraday Trans., 93*, 4159 (1997).

25. Saladin, F.; Forss, L.; Kamber, I., "Photosynthesis of CH_4 at a TiO_2 surface from gaseous H_2O and CO_2", *J. of the Chem. Soc.-Chem. Comm.,* 5, 533(1995).

26. Shicheng Yan, He Yu, Nanyan Wang, Zhaoshen Li and Zhiqang Zou, "Efficient conversion of CO_2 and H_2O into hydrocarbon fuel over ZnAl2O4- modified mesopourous ZnGaNO under visible light irradiation, *Chemical Communications*, issue 7, 1048 (2012)

27. Taniguchi, I. " Electrochemical and photoelectrochemical reduction of carbon dioxide"**,** *Modern Aspects of Electochemistry*, *20*, 327(1989).

28. Xu, Z., Lai, E., Shao-Horn, Y. Hamad-Schifferli, K., " Compositional dependence of the stability of AuCu alloy nanoparticles", Chem. Commun., 48, 5626 (2012).

29. Cunyu Zhao, Lianjun Liu, Qianyi Zhang, Jun Wang, and Ying Li, "Photocatalytic conversion of CO_2 and H_2O to fuels by nanostructured Ce-TiO_2/SBA-15 composites", Catalysis Science & Technology, issues 12, 2558 (2012)